ELSEVIER

Biochimica et Biophysica Acta 1527 (2001) 11–19

BIOCHIMICA ET BIOPHYSICA ACTA
BBA

www.bba-direct.com

In situ analysis of mineral content and crystallinity in bone using infrared micro-spectroscopy of the ν_4 PO_4^{3-} vibration

Lisa M. Miller [a,*], Vidyasagar Vairavamurthy [a], Mark R. Chance [a], Richard Mendelsohn [b], Eleftherios P. Paschalis [c], Foster Betts [c], Adele L. Boskey [c]

[a] *Albert Einstein Center for Synchrotron Biosciences, National Synchrotron Light Source, Building 725 D, Brookhaven National Laboratory, Upton, NY 11973-5000, USA*

[b] *Department of Chemistry, Rutgers University, Newark, NJ, USA*

[c] *Mineralized Tissues Research Section, Hospital for Special Surgery, New York, NY, USA*

Received 21 July 2000; received in revised form 1 December 2000; accepted 9 January 2001

Abstract

Measurements of bone mineral content and composition in situ provide insight into the chemistry of bone mineral deposition. Infrared (IR) micro-spectroscopy is well suited for this purpose. To date, IR microscopic (including imaging) analyses of bone apatite have centered on the ν_1,ν_3 PO_4^{3-} contour. The ν_4 PO_4^{3-} contour (500–650 cm^{-1}), which has been extensively used to monitor the crystallinity of hydroxyapatite in homogenized bone samples, falls in a frequency region below the cutoff of the mercury–cadmium–telluride detectors used in commercial IR microscopes, thereby rendering this vibration inaccessible for imaging studies. The current study reports the first IR micro-spectroscopy spectra of human iliac crest cross sections in the ν_4 PO_4^{3-} spectral regions, obtained with a synchrotron radiation source and a Cu-doped Ge detector coupled to an IR microscope. The acid phosphate (HPO_4^{2-}) content and mineral crystallite perfection (crystallinity) of a human osteon were mapped. To develop spectra–structure correlations, a combination of X-ray powder diffraction data and conventional Fourier transform IR spectra have been obtained from a series of synthetic hydroxyapatite crystals and natural bone powders of various species and ages. X-ray powder diffraction data demonstrate that there is an increase in average crystal size as bone matures, which correlates with an increase in the ν_4 PO_4^{3-} FTIR absorption peak ratio of two peaks (603/563 cm^{-1}) within the ν_4 PO_4^{3-} contour. Additionally, the IR results reveal that a band near 540 cm^{-1} may be assigned to acid phosphate. This band is present at high concentrations in new bone, and decreases as bone matures. Correlation of the ν_4 PO_4^{3-} contour with the ν_2 CO_3^{2-} contour also reveals that when acid phosphate content is high, type A carbonate content (i.e., carbonate occupying OH^- sites in the hydroxyapatite lattice) is high. As crystallinity increases and acid phosphate content decreases, carbonate substitution shifts toward occupation of PO_4^{3-} sites in the hydroxyapatite lattice. Thus, IR microscopic analysis of the ν_4 PO_4^{3-} contour provides a straightforward index of both relative mineral crystallinity and acid phosphate concentration that can be applied to in situ IR micro-spectroscopic analysis of bone samples, which are of interest for understanding the chemical mechanisms of bone deposition in normal and pathological states.

1. Introduction

Mineral features such as crystallite size and perfection (crystallinity), phosphate content, carbonate content, and mineral environment may be altered substantially as a function of tissue type, age, and pathology. Bone diseases such as osteogenesis imperfecta [1], osteomalacia [2], osteoporosis [3], osteopetrosis [4], and osteoarthritis [5] are characterized by abnormal tissue mineral content, deposition, and/or turnover.

Techniques traditionally used to study bone tissue, namely X-ray diffraction, nuclear magnetic resonance, electron spin resonance, and Fourier transform infrared (FTIR) spectroscopy, while permitting identification of the nature of the mineral phases present, provide neither spatially-resolved analysis of the various mineral phases, nor permit determination of the relative amounts of mineral and matrix present [6]. IR micro-spectroscopy permits chemical analysis of the organic and mineral components of bone [7] such that specific regions of the tissue can be analyzed with spatial resolution approaching the diffraction limit (3–20 μm), making this technique beneficial for understanding mechanisms of abnormal mineral deposition in bone disease.

* Corresponding author. Fax: +1-631-344-3238;
E-mail: lmiller@bnl.gov

0304-4165/01/$ – see front matter
PII: S0304-4165(01)00093-9

Following the initial demonstration of the feasibility of the approach [7], IR spectroscopy and micro-spectroscopy of bone have been used extensively to examine protein content [8,9], phosphate [10–13] and carbonate [14,15] content and environment, and mineral crystallinity [16–18]. Curve-fitting of the ν_1, ν_3 PO_4^{3-} contour (900–1200 cm^{-1}) reveals a variety of components assigned to apatitic phosphate and acid phosphate in environments of varying crystallinity [11]. Subtle changes in this broad contour are detectable as a function of bone crystal maturity [10]. For example, a component at 1145 cm^{-1}, which is assigned to acid phosphate, decreases as bone matures [13]. Also, the 1030/1020 cm^{-1} intensity ratio, which is an index of crystal size/perfection, increases as bone matures [11]. This parameter has been very useful for recent IR micro-spectroscopic imaging of bone [19,20].

Acid phosphate content and crystallinity can also be obtained from the ν_4 PO_4^{3-} spectral region (500–650 cm^{-1}). This contour can be fit to fewer components [12] than the ν_1,ν_3 contour, thereby simplifying curve-fitting analysis. However, the ν_4 PO_4^{3-} contour falls in a frequency region below the cutoff of the mercury-cadmium-telluride detectors used in commercial IR microscopes, thereby rendering this vibration generally inaccessible for imaging studies. To circumvent this problem, we recently described the use of a synchrotron infrared microscope coupled to a Cu-doped Germanium detector, which extends the collectable infrared range to 4000–400 cm^{-1} [21–23]. Through a 10-μm aperture, the synchrotron infrared source is 1000 times brighter than a conventional globar source. This high brightness permits collection of high quality data with a spatial resolution at the diffraction limit [24]. Since the ν_4 PO_4^{3-} contour is lower in frequency, the diffraction-limited spatial resolution is approximately twice that of the ν_1,ν_3 contour. However, the simplified data analysis and complementary information attainable from this contour make it a valuable region for infrared analysis.

In the present study, synchrotron IR micro-spectroscopy is used to monitor crystallinity and acid phosphate content in bone based on examination of the ν_4 PO_4^{3-} region. To develop spectra–structure correlations, a group of homogenized bone and synthetic hydroxyapatite samples are analyzed using conventional IR spectroscopy. Average crystal size/perfection (crystallinity) is determined from X-ray powder diffraction. These results are correlated with parameters derived from the corresponding IR spectra. Also, acid phosphate content [12] and carbonate content and environment [14] are determined in these samples. This set of trends is then applied to in situ IR micro-spectroscopic analysis of bone samples. The ability to measure relative bone mineral content and composition from within different regions of individual bone samples provides insight into the chemistry of how bone mineral is deposited in a single species.

2. Experimental methods

2.1. Materials

Bone samples for IR micro-spectroscopy were prepared from human iliac crest biopsies obtained from the Pathology Department at the Hospital for Special Surgery under an IRB approved protocol. The original specimen was obtained (for diagnostic reasons) from the left femur of a 28-year-old man diagnosed as osteopetrotic based on radiologic and histologic data. Animal bones were from specimens sacrificed for other purposes. Tissues included a 7-day mouse femur, a 7-week healing rabbit callus (before and after chloroform-methanol extraction to remove lipids), a baby rat femur, and calvaria and rib from a fetal calf.

2.2. X-ray powder diffraction

X-ray diffraction patterns were recorded on a Siemens D500 powder diffractometer (Iselin, NJ). The samples were ground to obtain a relatively uniform particle size, placed into an aluminum sample holder and scanned in 0.05° intervals between 20° and 37° (2θ) using Ni-filtered Cu–Kα radiation with a minimum of 8000 counts/interval.

2.3. Infrared spectroscopy

KBr pellets were prepared by mixing 10 mg of bone powder with 500 mg of KBr in a mortar and pestle and pressing the pellet in a 13 mm KBr pellet die (McCarthy Scientific Co., Fullerton, CA). FTIR spectra were collected on a Nicolet Magna 560 FTIR instrument equipped with a KBr beamsplitter and DTGS-polyethylene detector. For each sample, 128 scans were collected at 4 cm^{-1} resolution. For each spectrum, Savisky–Golay second-derivative analysis [25] was used (2nd-order polynomial, 5-point convolution) to determine the peak frequencies of all of the ν_4 PO_4^{3-} and ν_2 CO_3^{2-} region components. The ν_4 PO_4^{3-} region was first baseline-corrected using a cubic polynomial line fit, which was done to remove any contribution from the broad, underlying collagen band. A cubic polynomial baseline fit was also performed on the ν_2 CO_3^{2-} contour, in order to removed the sloping background from the ν_1,ν_3 PO_4^{3-} band. All curve-fitting was performed (Grams 32, Galactic Industries, Salem, NH) using Gaussian peak-fit components. The number of components was defined by second derivative analysis. The frequency of each peak component was confined to ± 2 cm^{-1} from the second derivative position and peak widths were restricted to ≤ 25 cm^{-1}, except for the broad HPO_4^{2-} component, which was restricted to ≤ 45 cm^{-1}. For the ν_2 CO_3^{2-} fit, four components were identified: 878, 871, 866, and 855 cm^{-1}. The weak, broad band at 855 cm^{-1} has been attributed to the P-OH stretch (ν_3 mode) of acid

phosphate [12] and can be directly correlated with the ν_4 mode near 530 cm^{-1} (data not shown). This component was necessary for a proper fit of the experimental data, but it was removed from the ν_2 CO_3^{2-} analysis.

2.4. Infrared micro-spectroscopy

Human bone samples were prepared as described previously [11]. A 5-μm-thick section was cut from the tissue block with a diamond saw. The bone section was placed between two KBr windows (13 mm diameter×2 mm thick). This sandwich assembly was mounted in a compression cell (Spectra Tech, Shelton, CT). IR spectra were recorded using a Spectra Tech Irμs Fourier transform infrared microscope, equipped with a motorized *x–y* mapping stage and Cu-doped Ge detector (Infrared Laboratories, Tucson, AZ). The microscope was modified such that the internal (globar) source was replaced by synchrotron infrared light at Beamline U4-IR at the National Synchrotron Light Source at Brookhaven National Laboratory. A digital camera was mounted to the microscope to enable optical imaging and recording of the regions probed with the infrared microscope. Spectra were collected in transmission mode, 128 scans per point, at 4 cm^{-1} resolution using Atlμs software (Nicolet Instruments, Madison, WI). The redundant apertures were set at 12×12 μm and spectra were collected in 10-μm steps across the osteon. The area map was 20×25 points, corresponding to an area 200×250 μm^2.

To correct for possible small variations in sample thickness, all data are expressed as ratios. The absorbance intensity ratios for each point in the map were exported from Atlμs as a three-column ASCII file and imported into Microcal Origin 5.0 (Microcal Software, Northampton, MA) for plotting. Matrices and contour plots were generated from the *x*,*y* map coordinates and absorbance intensity ratio (*z*) values.

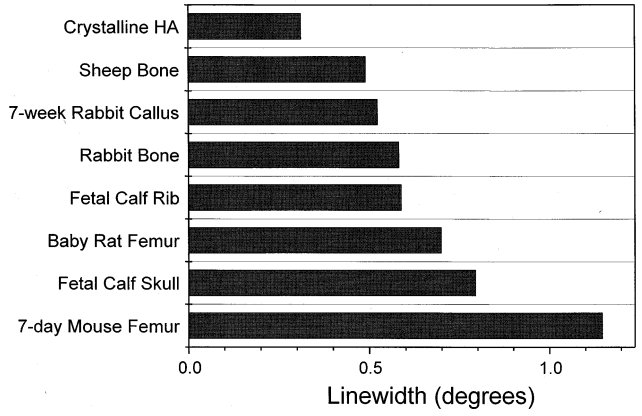

Fig. 1. X-ray powder diffraction linewidths (in degrees) for the [002] reflection of several different natural and synthetic apatite samples. Sample preparation and data collection are described in the text.

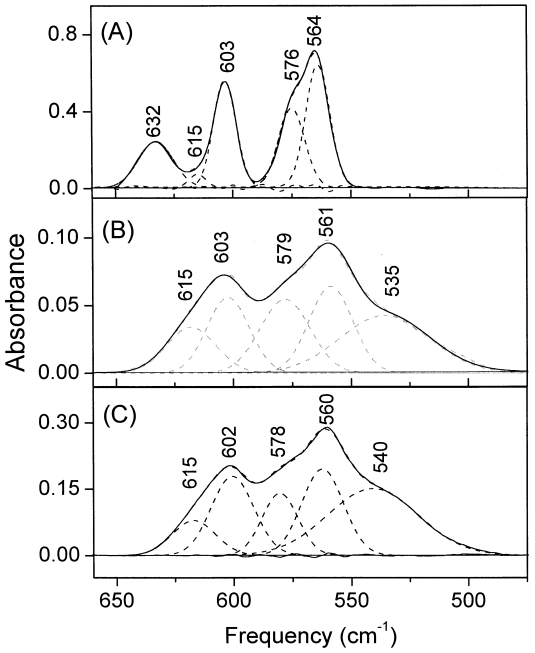

Fig. 2. Infrared spectra of the ν_4 PO_4^{3-} region for (A) highly crystalline synthetic apatite, (B) rabbit bone, and (C) 7-day-old mouse femur. Curve-fitting analysis was used to identify five components in the contour for both bone and synthetic hydroxyapatite. Samples were ground in a mortar and pestle with KBr and pressed into a pellet. Two hundred and fifty-six scans were collected at 4 cm^{-1} resolution.

3. Results and discussion

3.1. Spectra–structure correlation

A series of homogenized bone samples from several species of various ages were analyzed by X-ray powder diffraction. The width of an X-ray diffraction line represents a measure of the average bone crystallite size, perfection, and ordering (i.e., crystallinity) in a particular diffraction plane [26], where narrower linewidths indicate increased crystallinity. In Fig. 1, the *c*-axis [002] reflection linewidths at half the maximum height (in degrees) are plotted for all samples and arranged in decreasing order. It can be seen that, in general, the linewidth decreases as the bone matures. For example, the linewidth broadening from a 7-day-old mouse femur is larger than from a mature rabbit bone. In addition to the [002] reflection, linewidths from five other reflections were obtained. The ranks vary slightly for different reflections, suggesting that other factors, possibly including crystal habit, affect the linewidths. In practice, the [002] reflection is the only reflection that does not overlap other peaks and does not require curve-fitting. This unique reflection, which provides an index of *c*-axis size, is probably the easiest to use for sorting bone crystallinity.

Fig. 2 compares IR spectra in the ν_4 PO_4^{3-} region of highly crystalline hydroxyapatite, mature bone (rabbit bone), and young bone (7-day mouse femur). Five components are visible in these spectra and also the other six

Table 1
Position of bands from second-derivative analysis of the infrared data from several mineralized tissue samples

Sample	Band position					
7-Day mouse femur		614.9	601.8	578.2	560.0	540.0
Fetal calf skull		614.1	602.7	577.9	559.9	538.0
Baby rat femur		616.9	601.7	578.0	559.1	532.2
Fetal calf rib		616.2	603.2	579.1	560.8	541.9
Rabbit bone		615.4	602.9	578.9	560.9	535.2
7-Week rabbit callus		613.6	602.4	578.2	560.1	540.9
Sheep bone		615.2	602.6	577.8	561.2	537.6
Crystalline hydroxyapatite	632.5	615.0	603.2	575.8	564.4	

samples examined (Table 1). In general, the low site symmetry of the PO_4^{3-} tetrahedron splits the ν_4 PO_4^{3-} contour into three components. In apatitic PO_4^{3-}, these peaks fall near 600, 573, and 560 cm^{-1} [12,27]. In addition, a broad band centered between 530 and 540 cm^{-1} has been observed in both synthetic and biological apatites and assigned to acid phosphate (HPO_4^{2-}) in the mineral lattice [12,27]. This peak is much more intense in the young bone and decreases in mature bone and in highly crystalline synthetic apatite.

In Fig. 3, trends in the ν_4 PO_4^{3-} IR curve-fitting results for all of the homogenized bone samples are plotted as a function of the [002] diffraction linewidth. As a fraction of the total area, Fig. 3 illustrates a dramatic increase in the intensity of the 540 cm^{-1} component, and decreases in the peak intensities at 563, 575, and 603 cm^{-1} as crystallinity decreases. Linear correlations (R values) between the diffraction linewidths and IR absorbances are indicated in the figure caption. Positive correlations represent increases in infrared intensity with decreased linewidth (i.e., increased bone maturity).

It is well established from the ν_1,ν_3 PO_4^{3-} region (950–1200 cm^{-1}) that the apatite environment in newly deposited bone mineral is considerably nonstoichiometric, where labile, surface carbonate (CO_3^{2-}) and acid phosphate (HPO_4^{2-}) concentrations are high [11,13]. As bone ages or matures, crystal size and perfection increase and the apatite environment can become more stoichiometric. Both the ν_4 PO_4^{3-} data presented here and by Glimcher and coworkers [12] support these findings. As Fig. 3 illustrates, there is an increase in the fractional intensity of the band at 540 cm^{-1} as linewidth increases. Also as linewidth increases, the fractional intensities of the normal apatitic bands at 563, 575, and 603 cm^{-1} decrease (Fig. 3). These

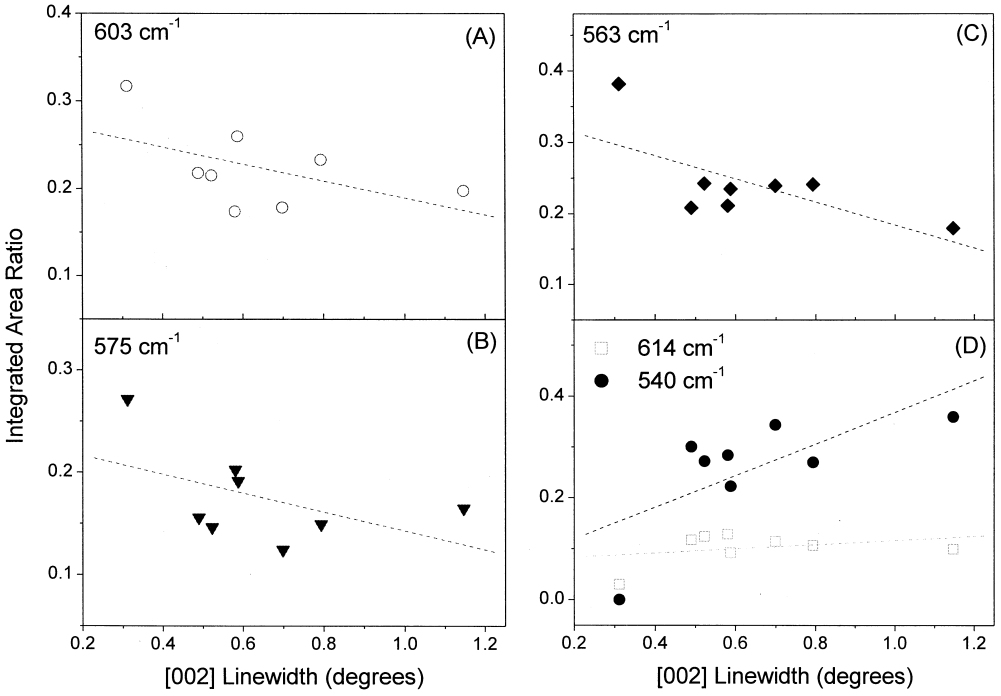

Fig. 3. From the curve-fit data, integrated area ratios were calculated for each component as a function of the overall integrated intensity of the ν_4 PO_4^{3-} band. These ratios are plotted for the (A) 603 cm^{-1} ($R=-0.546$; slope = 0.11 (0.07)), (B) 575 cm^{-1} ($R=-0.567$; slope = 0.11 (0.07)), (C) 563 cm^{-1} ($R=-0.770$; slope = 0.19 (0.07)), and (D) 614 cm^{-1} (slope = −0.05 (0.05)) and 540 cm^{-1} ($R=0.763$; slope = 0.35 (0.13)) components. The 540 cm^{-1} component increases and the 603, 575, and 563 cm^{-1} components decrease as linewidth increases, i.e., as bone crystal size decreases. Within the error of the data, the 615 cm^{-1} component remains constant.

results indicate that as bone matures, acid phosphate content is lost and the apatite 'perfection' increases. Within the error of the data, the band at 615 cm^{-1} remains small in intensity and of constant width. This band has been attributed to labile PO_4^{3-} in a poorly crystalline apatitic environment [12]. Thus for the samples that we have examined, there always remains a small fraction of labile PO_4^{3-} ($\sim$10%) at varying levels of bone maturity.

In addition to acid phosphate substitution into the hydroxyapatite lattice, bone mineral also contains a considerable amount of carbonate, up to 4% or 5% by weight [30]. In infrared spectra of bone, the $\nu_2CO_3^{2-}$ contour consists of three components attributable to Type A carbonate (878 cm^{-1}), Type B carbonate (871 cm^{-1}), and unstable carbonate (866 cm^{-1}) [14,15,28]. Type A and Type B carbonates represent carbonate substitution into the OH^- and PO_4^{3-} sites in the hydroxyapatite lattice, respectively, where the main carbonate location appears to be in the PO_4^{3-} location (Type B carbonate) [29]. By curve-fitting the $\nu_2CO_3^{2-}$ infrared contour, we have determined the relative site of carbonate substitution for all of the homogenized bone samples. First, we find a positive correlation between the unstable carbonate location (866 cm^{-1} component) and the acid phosphate content (538 cm^{-1} component) (Fig. 4), both of which are high in young bone [14]. The high concentration of unstable carbonate in young bone is consistent with the presence of labile, surface carbonate. As bone matures and average crystal size increases, the CO_3^{2-} ions settle into the two anionic sites of the apatite structure [15], where the overall degree of substitution is highly dependent upon many factors, such as bone species, strain, and type. Fig. 5 illustrates trends in Types A and B $\nu_2CO_3^{2-}$ components for all of the homogenized bone samples as a function of the [002] diffraction linewidth. The data demonstrate that the fraction of Type A carbonate decreases and the fraction of Type B carbonate increases as diffraction linewidth increases. This can be understood as an evolution of the maturing crystal toward stoichiometry. When a bivalent ion, such as CO_3^{2-} or HPO_4^{2-}, substitutes into a trivalent PO_4^{3-} site, the result is a loss of a negative charge. In order to restore neutrality to the crystal lattice, one Ca^{2+} cationic vacancy and one monovalent (OH^-) anionic vacancy are created. Therefore, when CO_3^{2-} and/or HPO_4^{2-} content are high, A site substitution is reduced. As bone crystals mature, CO_3^{2-} and HPO_4^{2-} contents decrease and the A site substitution increases.

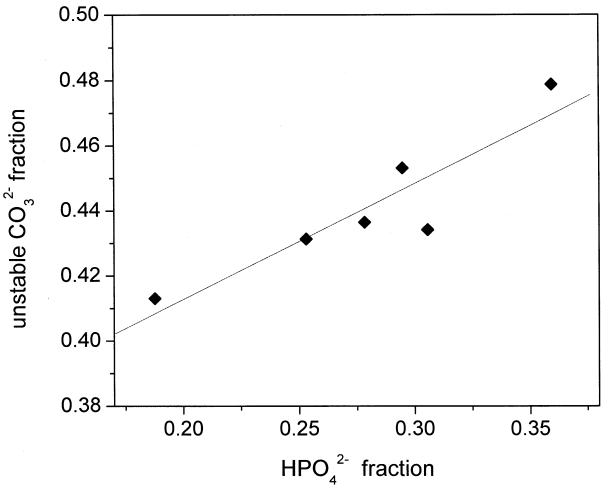

Fig. 4. Positive correlation ($R = 0.910$; slope = 0.36 (0.08)) between unstable, labile carbonate (866 cm^{-1}, integrated area ratio) and acid phosphate (540 cm^{-1}, integrated area ratio) content in the homogenized bone samples.

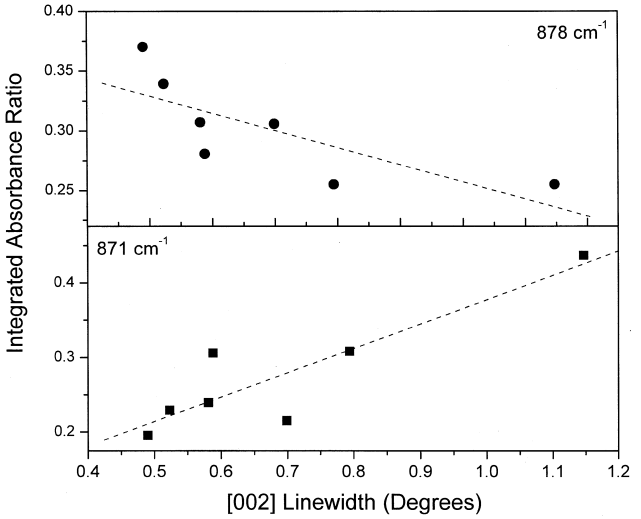

Fig. 5. Fractional area of total carbonate content for type A (■: 878 cm^{-1}) and type B (●: 871 cm^{-1}) carbonate in the homogenized bone samples as a function of diffraction linewidth. As linewidth increases, type A carbonate decreases ($R = -0.764$; slope = −0.14 (0.05)) and type B carbonate increases ($R = 0.892$; slope = 0.38 (0.07)).

3.2. In situ IR analysis

The use of second-derivative and curve-fitting analysis is required for accurate assignment of the ν_4 PO_4^{3-} components. It is clear that this curve-fitting can provide data on bone mineral structure analogous to that derived from the mid-infrared ν_1,ν_3 PO_4^{3-} data. However, in situ IR mapping of large regions of bone generates hundreds or thousands of spectra, making the curve-fitting protocols, as described here, difficult. Thus, a simplified means of extracting relative crystallinity and acid phosphate information using intensities from the ν_4 PO_4^{3-} would simplify IR data analysis of this region from mapping experiments of mineralized tissue. Such an analysis using IR array detectors has been described for the large data sets generated from the ν_1,ν_3 contour [19,20]. In Fig. 6, we demonstrate that the ratio of intensities at 603/563 cm^{-1} is linear with respect to crystallinity as determined by X-ray powder diffraction. This trend is understood from the following argument: The peak height at 563 cm^{-1} contains underlying contributions from the components at 563 and 538 cm^{-1} (see Fig. 2). The average width at half-maximum

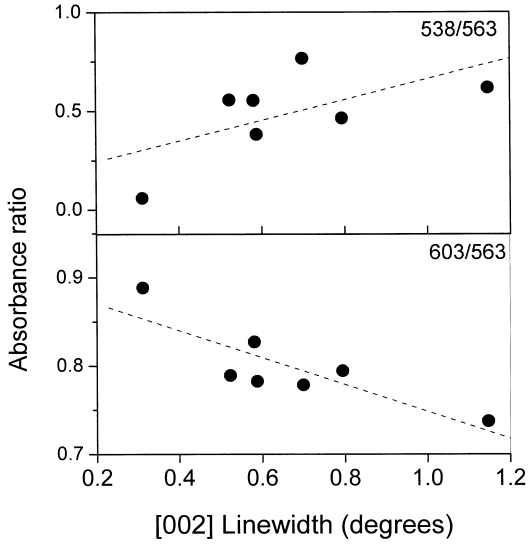

Fig. 6. Absorbance ratios for the peak heights measured at (A) 603/563 cm^{-1} ($R=-0.842$) and (B) 538/563 cm^{-1} ($R=0.610$) as a function of linewidth. No curve fitting or integrated intensities were measured for these ratios.

height of the 540 cm^{-1} band is 45 cm^{-1}, indicating (since the band shape is assumed to be symmetric) that the peak height of this component at 563 cm^{-1} is one-half its maximum height. Thus, the peak height at 563 cm^{-1} is equal to the height of the 563 cm^{-1} component plus one-half the height of the 540 cm^{-1} component. This value is found to be independent of X-ray linewidth (Fig. 7). This result supports the curve-fitting analysis, which demonstrated that the rate of increase of the 563 cm^{-1} component is one-half the rate of decrease of the 540 cm^{-1} component as linewidth decreases (Fig. 3).

Similarly, the peak height at 603 cm^{-1} contains contributions from the components at 615 and 603 cm^{-1}. The average width at half-maximum height of the 615 cm^{-1} band is 25 cm^{-1}, so by the same argument made above, the peak height at 603 cm^{-1} is equal to the height of the 603 cm^{-1} component plus one-half the height of the 615 cm^{-1} component. This value increases linearly with increasing crystallinity (Fig. 7) because, as mineralization increases, the amount of apatitic phosphate increases. Therefore, the 603/563 cm^{-1} ratio provides a measure of average crystallinity.

From Table 1, it can be seen that the average peak position of the acid phosphate band is 538 ± 4 cm^{-1}. From Fig. 2, it can be seen that the peak height at 538 cm^{-1} provides a direct measure of acid phosphate content, since the closest (563 cm^{-1}) component is 33 cm^{-1} higher in frequency and has an average band width of 25 cm^{-1}. Conversely, the peak height at 563 cm^{-1} contains contributions from the components centered at 563 and 538 cm^{-1}. Since 563 cm^{-1} peak intensity remains constant with respect to linewidth (Fig. 7), plotting the peak height ratio 538/563 cm^{-1} provides a measure of the acid phosphate content in the bone sample (Fig. 6).

Although these X-ray and IR studies were performed on bone from numerous species of varying ages, significant trends are observed in crystallinity and acid phosphate content as a function of bone age. The goal of this project is to identify and characterize these trends so that they can be applied to in situ IR micro-spectroscopic analysis of bone samples. The ability to measure relative bone mineral content and composition in situ provides insight into the chemistry of how bone mineral is deposited in a single species. To illustrate this point, an infrared area map was collected from an area of trabecular bone containing an osteon as seen in Fig. 8. Osteons are created by the combined effects of (1) the tunnel-like erosion of old bone by osteoclasts and (2) the layer-by-layer deposition of new bone by osteoblasts. Thus, on a relative scale, the bone located at the center of an osteon is less mature than bone at its periphery. The infrared maps in Fig. 8 represent the acid phosphate content (538/563) and crystallinity (603/563) ratios. The ν_4 PO_4^{3-} region of individual spectra selected every 10 μm from the osteon center can be seen in Fig. 9A. From the center of the osteon to the periphery, notice that the acid phosphate content decreases and crystallinity increases. As expected, these spectra represent bone that is more mature at the periphery of the osteon. These trends are also plotted in Fig. 9B, where we see a marked change in bone maturity within the first 30 μm of new bone growth. Fig. 10 shows the distribution of crystallinity and acid phosphate content ratios obtained from the entire area map. The average crystallinity and acid phosphate content ratios are 0.88 ± 0.20 and 0.26 ± 0.10, respectively. Thus, by 30 μm from the center of the osteon, the bone has reached a maturity equal to the average value obtained from the entire mapped area.

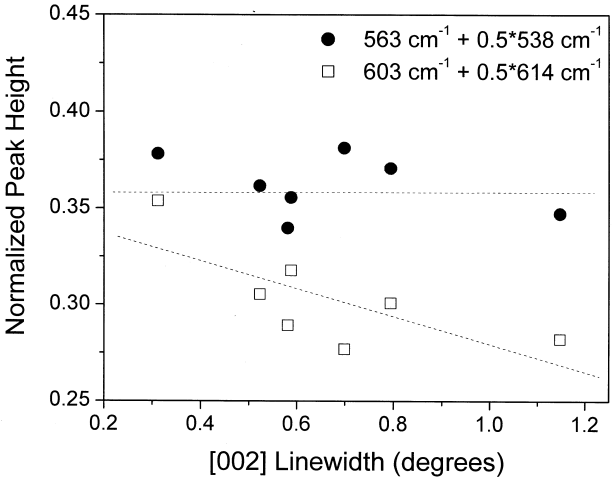

Fig. 7. The actual peak heights at 603 and 563 cm^{-1} can be expressed as sums of the following curve-fit component peak heights: 563 cm^{-1} (●) = (563 cm^{-1} + 1/2 × 540 cm^{-1}) and 603 cm^{-1} (□) = (603 cm^{-1} + 1/2 × 614 cm^{-1}) These values are normalized to the sum of the peak heights from the five curve-fit components and plotted as a function of linewidth. The peak height at 563 cm^{-1} remains constant as a function of linewidth and the peak height at 603 cm^{-1} decreases linearly with linewidth ($R=-0.719$).

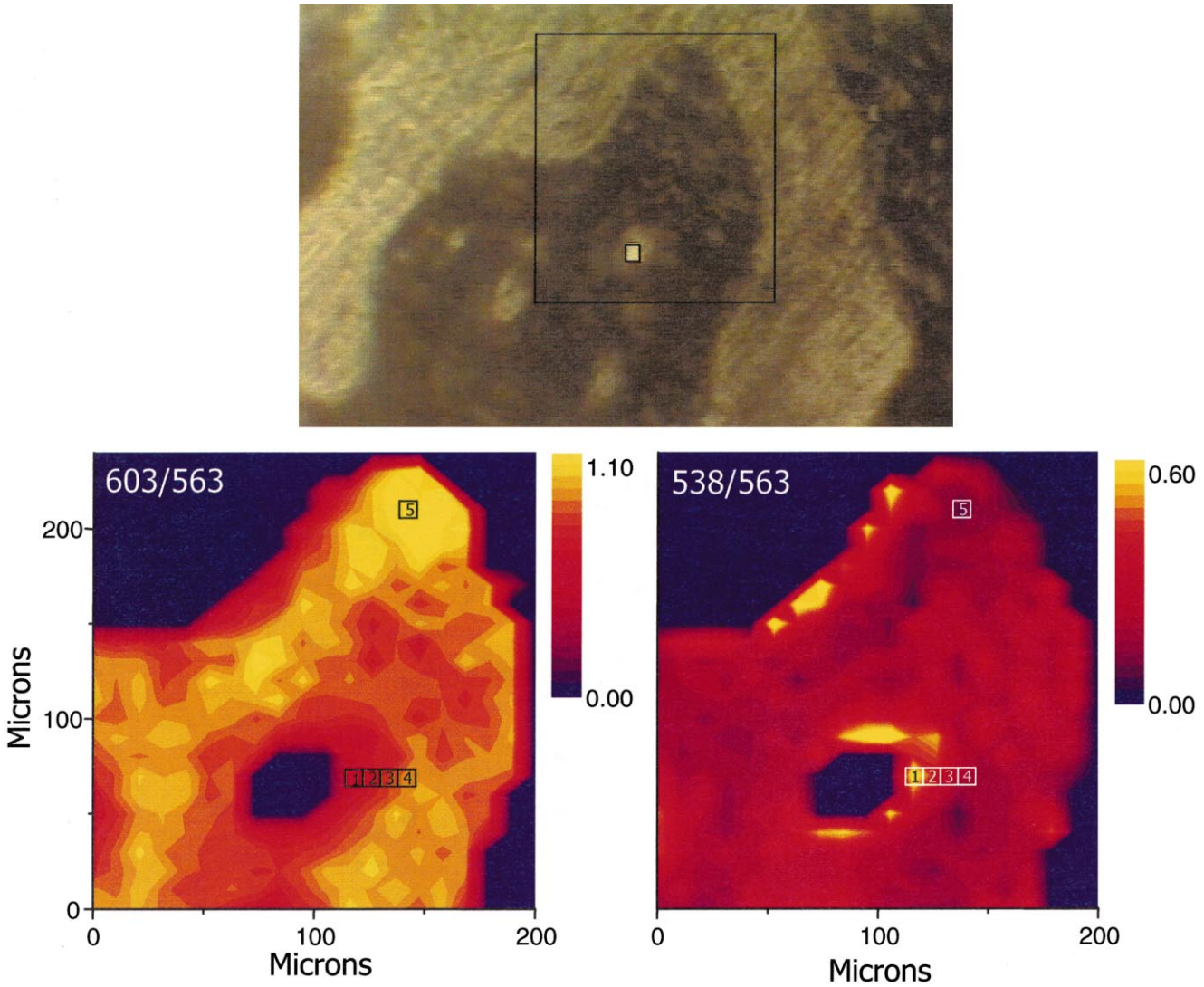

Fig. 8. Optical and infrared images of human, osteopetrotic, trabecular bone. Data were collected at Beamline U4IR at the NSLS using a Spectra Tech Irμs infrared microscope and a Cu-doped Ge detector (Infrared Laboratories). Apertures were set to 12×12 μm and 128 scans were collected at 4 cm^{-1} resolution. Infrared images were generated by plotting peak height ratios of (left) 603/563 cm^{-1} and (right) 538/563 cm^{-1}.

Finally, from the IR area maps, it can generally be concluded that where crystallinity is high, acid phosphate content is low. An additional spectrum is shown from the tip of the trabecular 'finger' (dotted line in Fig. 9A). The crystallinity ratio is extremely high and the acid phosphate content ratio is low, representative of mature bone. Conversely, spectra collected along the edge of the trabecular 'finger' have high acid phosphate concentrations and lower crystallinity.

These results generally confirm recent IR microscopic imaging investigations which mapped the spatial distributions of parameters derived from the ν_1,ν_3 PO_4^{3-} contour [19,20]. With a synchrotron IR source, coupled with a Cu-doped Ge detector, these studies are now feasible in the ν_4 spectral region, and complement those currently under way (with array detector-imaging technology) in the ν_1,ν_3 domain. In the future, we plan to extend prior comparative studies [19,20] of overall distributions of mineral crystallinity in normal vs. diseased states of bone. By doing so, we hope to identify any mechanical and/or physiological abnormalities that occur in bone mineral deposition leading to bone disease.

4. Conclusions

In summary, the ν_4 PO_4^{3-} region of the infrared spectrum of bone contains information about crystallinity and acid phosphate content in the sample. By comparing spectra of bone to synthetic hydroxyapatite, we have confirmed the existence of an acid phosphate component near 540 cm^{-1} [10,12]. By combining X-ray powder diffraction linewidths and infrared data, we find that the peak height ratio of 603/563 cm^{-1} is directly related to crystallinity. Using these assignments, relative HPO_4^{2-} content and mineral crystallinity can be probed in a single

species in situ using IR microspectroscopy of the ν_4 PO_4^{3-} region. This is demonstrated for the first time in an in situ analysis of a human bone sample. Acid phosphate content and crystallinity are found to be inversely related, i.e., high acid phosphate content and low crystallinity are features of young (immature) bone. In addition, analysis of a maturing human osteon confirms that the most dramatic changes in osteon composition occur within 30 μm of the osteon center, i.e., within 30 μm of the site of new bone growth.

Acknowledgements

We would like to thank G.L. Carr and G.P. Williams of the National Synchrotron Light Source, Brookhaven National Laboratory for their valuable input into this collaborative project and for the use of Beamline U4IR. We would also like to acknowledge the technical support of Michael Sullivan. This work is supported by the American Federation for Aging Research, A98087 (L.M.M.), the National Institutes of Health Biomedical Technology Program, P41-RR-01633 (M.R.C.), and the National Institutes of Health AR- 41325 (A.L.B., R.M.). The NSLS is supported by the United States Department of Energy under contract DE-AC02-98CH10886.

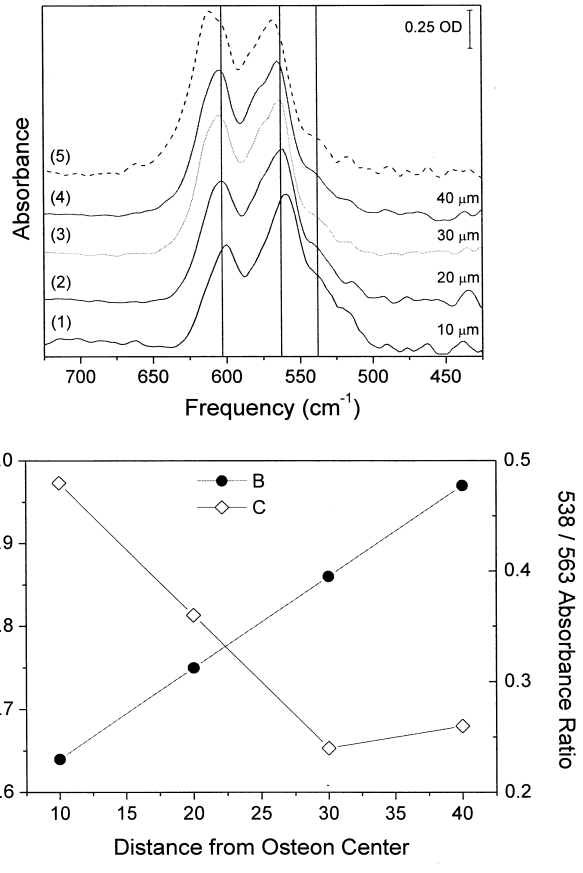

Fig. 9. (A) Infrared spectra of the ν_4 PO_4^{3-} contour at individual points collected as illustrated in Fig. 8. The first four points were collected from the center to the periphery of an osteon. Vertical lines represent 538, 563, and 603 cm^{-1}. (B) Peak height absorbance ratios for (◇) 538/563 and (●) 603/563 from the above spectra as a function of distance from the osteon center. Both figures illustrate that from the center of the osteon to the periphery, crystallinity increases and acid phosphate content decreases.

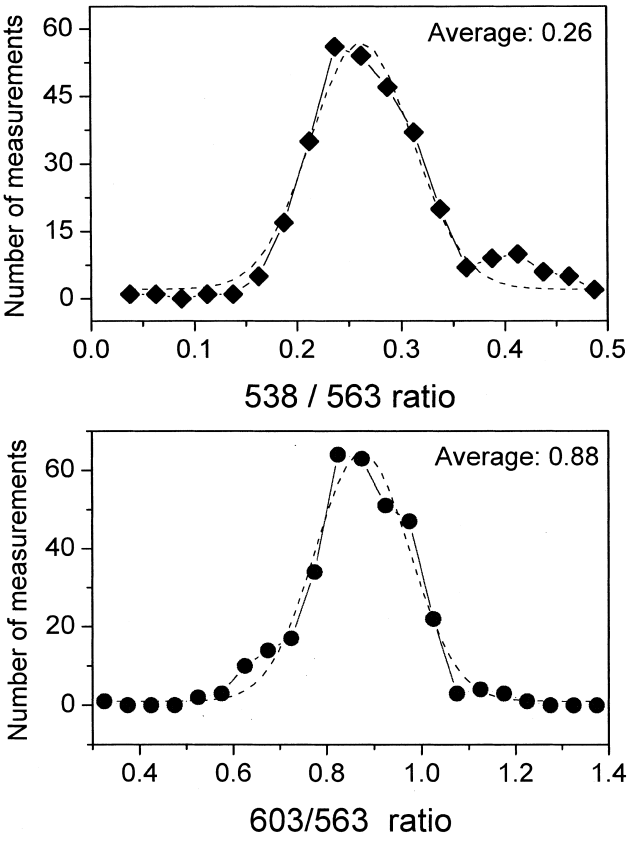

Fig. 10. Curves indicate distributions of (A) 538/563 cm^{-1} and (B) 603/563 cm^{-1} for the infrared map described in Fig. 8. Gaussian curve-fitting was performed on each normal distribution and the average acid phosphate content and the average crystallinity ratios were found to be 0.26 ± 0.10 and 0.88 ± 0.20, respectively.

References

[1] N.P. Camacho, L. Hou, T.R. Toledano, W.A. Ilg, C.F. Brayton, C.L. Raggio, L. Root, A.L. Boskey, J. Bone Miner. Res. 14 (1999) 264–272.
[2] A.L. Boskey, E.F. DiCarlo, H. Gilder, R. Donnelly, S. Wientroub, Bone 9 (1988) 309–318.
[3] C.A. Baud, J.M. Very, B. Courvoisier, Bone 9 (1988) 361–365.
[4] A.L. Boskey, S.C. Marks, Calcif. Tissue Int. 37 (1985) 287–292.
[5] L.M. Miller, D. Hamerman, M.R. Chance, C.S. Carlson, SPIE 3775 (1999) 104–112.
[6] A.L. Boskey, N. Pleshko, S.B. Doty, R. Mendelsohn, Cells Mater. 2 (1992) 209–220.
[7] R. Mendelsohn, A. Hassankhani, E. DiCarlo, A. Boskey, Calcif. Tissue Int. 44 (1989) 20–24.
[8] S.J. Gadaleta, N.P. Camacho, R. Mendelsohn, A.L. Boskey, Calcif. Tissue Int. 58 (1996) 17–23.
[9] E.P. Paschalis, O. Jacenko, B. Olsen, R. Mendelsohn, A.L. Boskey, Bone 19 (1996) 151–156.

[10] S.J. Gadaleta, E.P. Paschalis, F. Betts, R. Mendelsohn, A.L. Boskey, Calcif. Tissue Int. 58 (1996) 9–16.
[11] E.P. Paschalis, E. DiCarlo, F. Betts, P. Sherman, R. Mendelsohn, A.L. Boskey, Calcif. Tissue Int. 59 (1996) 480–487.
[12] C. Rey, M. Shimizu, B. Collins, M.J. Glimcher, Calcif. Tissue Int. 46 (1990) 384–394.
[13] C. Rey, M. Shimizu, B. Collins, M.J. Glimcher, Calcif. Tissue Int. 49 (1991) 383–388.
[14] C. Rey, B. Collins, T. Goehl, I.R. Dickson, M.J. Glimcher, Calcif. Tissue Int. 45 (1989) 157–164.
[15] C. Rey, V. Renugopalakrishnan, M. Shimizu, B. Collins, M.J. Glimcher, Calcif. Tissue Int. 49 (1991) 259–268.
[16] N. Pleshko, A.L. Boskey, R. Mendelsohn, Biophys. J. 60 (1991) 786–793.
[17] E.P. Paschalis, F. Betts, E. DiCarlo, R. Mendelsohn, A.L. Boskey, Calcif. Tissue Int. 61 (1997) 487–492.
[18] E.P. Paschalis, F. Betts, E. DiCarlo, R. Mendelsohn, A.L. Boskey, Calcif. Tissue Int. 61 (1997) 480–486.
[19] C. Marcott, R.C. Reeder, E.P. Paschalis, D.N. Tatakis, A.L. Boskey, R. Mendelsohn, Cell Mol. Biol. (Noisy-le-grand) 44 (1998) 109–115.
[20] R. Mendelsohn, E.P. Paschalis, A.L. Boskey, J. Biomed. Optics 4 (1999) 14–21.
[21] L.M. Miller, C.S. Carlson, G.L. Carr, G.P. Williams, M.R. Chance, SPIE 3153 (1997) 141–148.
[22] J.L. Bantignies, G.L. Carr, P. Dumas, L.M. Miller, G.P. Williams, Synchrotron Radiat. News 11 (1998) 31–36.
[23] L.M. Miller, C.S. Carlson, G.L. Carr, M.R. Chance, Cell. Mol. Biol. 44 (1998) 117–127.
[24] G.L. Carr, Vibrat. Spectrosc. 19 (1999) 53–60.
[25] A. Savitzky, M.J.E. Golay, Anal. Chem. 36 (1964) 1627.
[26] B.D. Cullity, in: Elements of X-Ray Diffraction, Addison Wesley, Reading, MA, 1967, p. 99.
[27] B.O. Fowler, E.C. Moreno, W.E. Brown, Arch. Oral Biol. 11 (1960) 477–496.
[28] C. Rey, V. Renugopalakrishnan, B. Collins, M.J. Glimcher, Calcif. Tissue Int. 49 (1991) 251–258.
[29] J.C. Elliot, A.W. Holcomb, R.A. Young, Calcif. Tissue Int. 37 (1985) 372–375.
[30] W.F. Neuman, M.W. Neuman, The Chemical Dynamics of Bone Mineral, University of Chicago Press, Chicago, 1958, p. 95.